Corrosion Inhibition of Carbon Steel in 0.5 M H_2SO_4 by New Reduced Schiff Base Ligand

Hojat Jafari[1] · Majid Rezaeivala[2] · Nader Mokhtarian[1] · Avni Berisha[3] · Elham Ameri[1]

Abstract

The effect of new reduced Schiff base ligand, named 2,2′-(((2,2-dimethylpropane-1,3-diyl)bis(azanediyl)bis(methylene) disphenol (RSH2), on the corrosion inhibiting of carbon steel in 0.5 M H_2SO_4 has been studied. The inhibitor effects on the corrosion behavior of the samples were determined at three different concentrations, 1.0, 1.5, and 2.0 mg L^{-1}. Weight loss, potentiodynamic polarization curves, AC impedance measurements, and atomic force microscopy were utilized to study the corrosion behavior of carbon steel in corrosive environment in the presence and absence of new ligand. Results showed that the inhibition occurs through adsorption of the inhibitors molecules on the metal surface. The inhibition efficiency was found to increase with increasing inhibitor's concentration. Potentiodynamic polarization data indicated that this compounds act as mixed-type inhibitors. The corrosion efficiency of RSH2 at an optimal concentration of 2 mg L^{-1} was 81. The adsorption of inhibitors followed the Langmuir isotherm. The value of free energy of adsorption in the presence of the corrosion inhibitor was around − 32 kJ mol^{-1}, which indicated chemisorption of the molecules. Powerful microscopy was used for the surface morphology studies. The DFT calculations have been demonstrated that the inhibitor is relatively flat-adsorbed on both sides of the phenyl rings.

1 Introduction

Corrosion is an exceedingly challenging and harmful progression that comprises the continuous and spontaneous degradation of metallic structures through chemical and/or electrochemical reactions with the ingredients of the environment [1–3]. Many industries, especially petroleum-based industries where metallic materials are extensively used, are badly affected by corrosion-related failures [4–6].

✉ Hojat Jafari
hojatjafari80@yahoo.com

✉ Majid Rezaeivala
mrezaeivala@hut.ac.ir

1 Department of Chemical Engineering, Islamic Azad University, Shahreza Branch, P.O. Box 311-86145, Shahreza, Iran

2 Department of Chemical Engineering, Hamedan University of Technology, Hamedan 65155, Iran

3 Department of Chemistry, Faculty of Natural and Mathematics Science, University of Prishtina, 10000 Prishtina, Kosovo

Many methods and strategies are developed to minimize the corrosion-related failures and subsequent cost of corrosion. Many methods of corrosion prevention have been developed but in the solution phase, the use of organic compounds, principally heterocyclic, is one of the most significant, effective, and economic methods [7, 8]. These compounds contain some structural features such as a combination of polar groups and conjugation in the form of aromatic ring, double and triple bonds through which they strongly interact with the metal surface [9–12]. Obviously, these electron dense centers are called as adsorption centers or adsorption sites. These compounds adsorb at the interface of environment and metal surface and build corrosion-protective film. The word "ecofriendly corrosion inhibitors" was talking about the compounds that are biocompatible, because these were organic origin. They were not affecting health and the environment in contending corrosion [13–15]. Literature investigation suggests that research and development on the synthesis, modification, characterization, and implementation of Shiff base as ecofriendly corrosion inhibitors are growing rapidly in the different fields of science, engineering, and technology. Barmatov and Hughes studied the

corrosion inhibition efficiency of the Schiff base, and its hydrolysis products on steel in HCl. All these compounds act as good inhibitors and they have similar inhibition efficiency at similar molar concentration [16]. Zhang et al. determined the inhibition efficiency of Schiff base-based cationic Gemini surfactants toward carbon steel in the corrosive medium by electrochemical impedance spectroscopy, potentiodynamic polarization, and weight loss measurements. These results reveal that these Gemini surfactants are efficient corrosion inhibitors for metal. [17] In terms of molecular parameters, Satpati et al. explained the variation in the inhibition efficiency of cinnamaldehyde and three different amino acids, using quantum mechanical calculation and molecular dynamics simulation.. It was found that all the three inhibitors impart appreciable extent of corrosion inhibition efficiency under the extreme [18]. Jafari et al. have tested two N_2O_4 Schiff base ligands for the corrosion inhibition of carbon steel in 0.5 M H_2SO_4 using potentiodynamic polarization and EIS methods. The results showed that two ligands behaved as a mixed inhibitor and the inhibition took place through adsorption of the compounds on the steel surface [19]. In this work, it is aimed to examine the corrosion rate and inhibition performance with and without the use of 2,2'- (((2,2-dimethylpropane-1,3-diyl)bis(azanediyl) bis(methylene)disphenol (RSH2) in 0.5 M H_2SO_4 solution. For this purpose, the weight loss, potentiodynamic polarization curves, DFT, and AC impedance measurements for carbon steel samples are used to determine the optimal concentrations of the inhibitor. The adsorption isotherm of the corrosion inhibitor on the carbon steel samples is investigated to determine the equilibrium constant and standard free energy. Finally, the surface morphology of the sample in 0.5 M H_2SO_4 with inhibitor and without inhibitor is studied using scanning electron microscopy (SEM) and atomic force microscopy (AFM) method.

2 Experimental Procedure

The first step in all corrosion tests is preparing of the test samples. Square carbon steel samples with an exposed area of 1 cm^2 were cooled in cold epoxy resin then polished with grade emery paper number 220 to 2000 and washing them with distilled water and acetone (its purity was 95% and trade mark was Xilong). After that, they were dried with air and kept as a working electrode in a desiccator until use. The samples were prepared from ST-37 carbon steel which had the chemical composition (wt. C: 0.61, Si: 0.23, Ni: 0.07, Mo: 0.08, Mn: 0.75, Cr: 0.1%w, Fe:Rest).

H_2SO_4 solution was prepared from 98% H_2SO_4 of Merck Product and distilled water. The compound named 2,2'- (((2,2-dimethylpropane-1,3-diyl)bis(azanediyl) bis(methylene)disphenol (RSH2) was prepared according to the described procedure [20, 21]. The concentration of inhibitors employed was 0.5, 1, 1.5, and 2 mg L^{-1}. Figure 1 shows the Schiff base ligand of this study.

Weight loss (mass loss) of the mild steel in the 0.5 M H_2SO_4 solution without and with RSH at 308 K with different immersion period (0 to 14 h). After the specified time, the steel samples are submerged from the 0.5 M H2SO4 solution and weight loss of steel sample was recorded. The protection efficiency of the corrosion inhibitor is calculated from the below equation [22]:

$$\text{Corrosion inhibition efficiency } (\%) = \frac{(W_1 - W_2)}{W_1} \times 100$$

(1)

where W_1 = unprotected steel weight loss, and W_2 = protected steel weight loss of the system.

Autolab device was used to perform potentiodynamic polarization tests. The tests were performed on a standard cell containing platinum foil (the immersed active area was 2×2 cm^2) as an auxiliary electrode and calomel as a reference electrode (EG&G Model 273). The experiments were performed at room temperature. At the beginning of each experiment, an interval of about 30 min was applied to stabilize the potential of the components in solution. From the potential range of about -800 to -200 mV compared to the open circuit potential and scan rate of 1 mV s^{-1}.

Electrochemical test was performed for steel samples after 30 min of immersion in the solutions. For this purpose, a three-electrode electrochemical cell including counter electrode (graphite), reference electrode (Calumel electrode), and working electrode (steel sample) is connected to a computer-controlled AutoLab potentiostat/galvanostat system (PGSTAT 302) and tested in open circuit potential in the frequency range of 100 kHz to 10 mHz with a peak amplitude of 10 mV A.C. .

Atomic forced microscopy was used to study the morphology of the samples surface. In this method, steel samples were immersed for 24 h in 0.5 M H_2SO_4 solution without inhibitor and also containing 2 mg of inhibitor at room
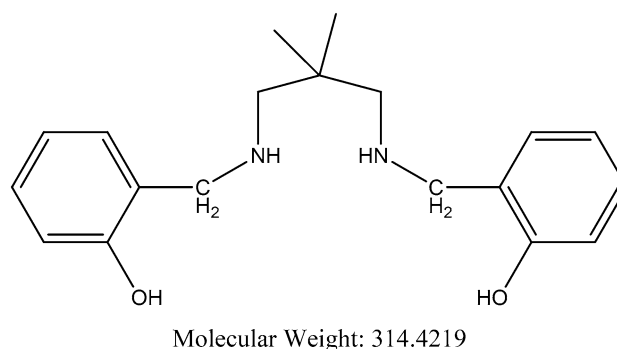

Molecular Weight: 314.4219

Fig. 1 Chemical structure of inhibitor

temperature. The samples were then removed from the solution and we washed them with distilled water and acetone, they were photographed by atomic force microscopy (AFM) NanoSurf easyscan2.

The FMOs were studied using the Materials Studio software program's DMol3 module. A double numerical basis set and polarization were used in conjunction with the M06-L [23–25] functional to improve the geometrical properties of all inhibitors in order to better understand electronic interaction and correlation (DNP) [26]. A shift in energy of less than 10–7 Ha was required for the self-consistent field to converge. The conductor-like screening model (COSMO) [27–29] was used in this investigation to account for the influence of the solvent – water.

The Material Studio program's Adsorption Locator tool was used to investigate potential interactions between the inhibitor molecules and the Fe (110) surface atoms. The interactions were investigated using a Monte Carlo (MC) method. A cell with the dimensions $1.986 \text{ nm} \times 1.986 \text{ nm} \times 1.419 \text{ nm}$, with a vacuum slab extending 3 nm beyond the cell's Fe (110) surface. The MC simulations were carried out by continuously loading the inhibitor molecules into a modeled cell, along with aqueous solutions of corrosive species such as H_2O (350), H_3O^+ (10), and SO_4^{2-} (5), and simulating the effects of these corrosive species using the Adsorption locator module in Material Studio. The target atoms for the MC simulation were particularly chosen from the topmost layer of the Fe (110) slab because it was thought to include plausible places for the inhibitor molecule's adsorption. The equilibrium adsorption configuration with the least amount of energy was studied and characterized as a consequence of the simulation's conclusion.

MD simulations are used to simulate inhibitor chemical adsorption on metal surfaces. Material Studio was used for the DFT, MC, and molecular dynamics simulations in this investigation. Compass was used to optimize the geometries of the inhibitor, water, sulfate, and hydronium in Material Studio's Forcite module [30–37]. Inhibitor molecule, 350 water molecules, and 10 hydronium + 5 sulfate ions were added to each system randomly. MD simulation is presented in this article in order to explore the interactions that take place between the metal surface of an inhibitor and aqueous sulfuric acid corrosion media. Following this, the slab is subjected to optimization. To begin, a cell of iron with a (110) plane was built using nine atom layers of thickness as its building blocks. The name "Fe" has been given to this surface (110). The simulations were done on the Fe (110) plane because of its dense structure and low energy surface [38, 39]. Following its development, the simulation box was geometrically altered to eliminate unfavorable chemical combinations and build an energetically minimal model for future simulations. A "smart" algorithm was used in the optimization process. The temperature and energy fluctuation curves remained constant as a result of optimization. Our next step was to use the widely used COMPASS forcefield and run MD simulations in Material Studio's Forcite module at 295 K with all Fe (110) atoms save the two top layers frozen (with a time step of 1.0 fs). The simulation acquired 0.8 ns [32, 33]. Using the trajectory of the MD simulation, the radial distribution function (RDF) was generated in order to predict how the inhibitor molecule adsorbs.

3 Results

3.1 Weight Loss Method

An important tool for preventing corrosion is the use of compounds with high efficiency, low cost, and low toxicity [40]. Figure 2 presents the results of the inhibition efficiency of RSH2 at 25 °C and various concentrations. As shown in the figure, the corrosion rate was increased significantly in the absence of the corrosion inhibitor over time. After 28 h of immersion of the carbon steel samples in the H_2SO_4 solution, the inhibition efficiency was higher than 80 in the absence of the inhibitor. The addition of the inhibitor reduced the corrosion rate. It is related to the adsorption of the reagent on the surface of the carbon steel samples. As can be seen, with an increase in the inhibitor concentration, the corrosion rate was decreased, and the inhibition efficiency was increased, reaching a constant value. This means that the values of the surface coverage and the corrosion efficiency were enhanced markedly by increasing the concentration of inhibitor. The optimal concentration of RSH2 was obtained 2 mg L^{-1}, as the corrosion rate and inhibition performance were not noticeably changed at higher concentrations. As shown in Fig. 2, the corrosion rate and inhibition efficiency after 28 h at 2 mg L^{-1} were 78%.
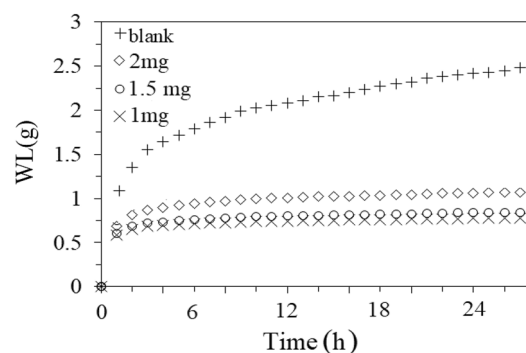

Fig. 2 Inhibition efficiency of the inhibitor at 25 °C

3.2 Potentiodynamic Polarization Diagram

Figure 3 shows the potentiodynamic polarization diagram of steel in 0.5 M H_2SO_4 without the presence of inhibitor and different concentrations of inhibitor. Electrochemical parameters including corrosion potential (E_{corr}), corrosion current intensity (I_{corr}) and anodic and cathodic Toefl slopes (β_a, β_c) are measured and are shown in Table 2. The degree of surface coverage (θ) and inhibitory efficiency (IE%) are calculated by the following equations [41, 42]:

$$\theta = \frac{I° - I}{I°} \tag{2}$$

$$IE\% = \frac{I° - I}{I°} \times 100 \tag{3}$$

$\dot{I}_{corr}$ and I_{corr} are the density of corrosion currents in solution without inhibitor and in the presence of inhibitor, respectively. As shown in Table 2, the corrosion current density decreases with increasing inhibitor concentration. Also, with increasing Schiff base concentration, both tofel anode and cathode slopes do not have a specific trend. This confirms that the inhibitor prevents corrosion by covering the active points on the metal surface [43]. The amount of corrosion potential in the presence of inhibitor is reduced compared to the solution without Schiff base and the corrosion potential decreases with increasing concentration of the inhibitor. Figure 3 shows the results of the polarization

test which confirms this. Considering that at low concentration, the corrosion potential is reduced compared to the solution without inhibitor. This inhibitor did not have an impressive effect on the anodic and cathodic tafel slopes. It can be concluded that the inhibitory function of Schiff base ligand reduced the exchange rate of anodic and cathodic reactions which have a greater effect on the cathode branch. However, as the inhibitor concentration increases, the corrosion potential moves to more negative values (Fig. 3), which indicate that as the inhibitor concentration increases, its effect on the cathode branch increases. According to Table 1, with increasing the ligand concentration, inhibition efficiency increased. The inhibitor was mixed type due to its effect on the anodic reaction of metal dissolution and the cathodic reaction of hydrogen and oxygen reduction. However, the effect on the cathodic reaction is more pronounced. In other words, the increase in anodic dissolution energy is less than the increase in hydrogen reduction energy. In addition, the corrosion potential changes slightly with increasing concentration, indicating a mixed mechanism [44–47].
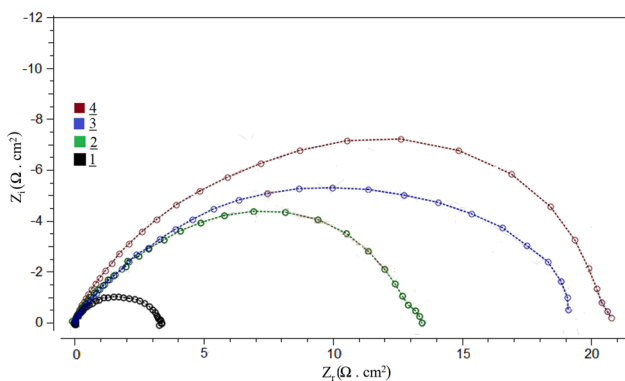
3.3 EIS Test

Figure 4 shows the Nyquist diagram in H_2SO_4 solution without inhibitor and at different concentrations of inhibitor. As shown in the Fig. 4, the radius of the semicircle increases with increasing concentration. This indicates that with increasing inhibitor concentration, the resistance to

Fig. 3 Tafel plots without and with corrosion inhibitor: blank (1), 1 (2), 1.5 (3), 2 (4) mg L^{-1}
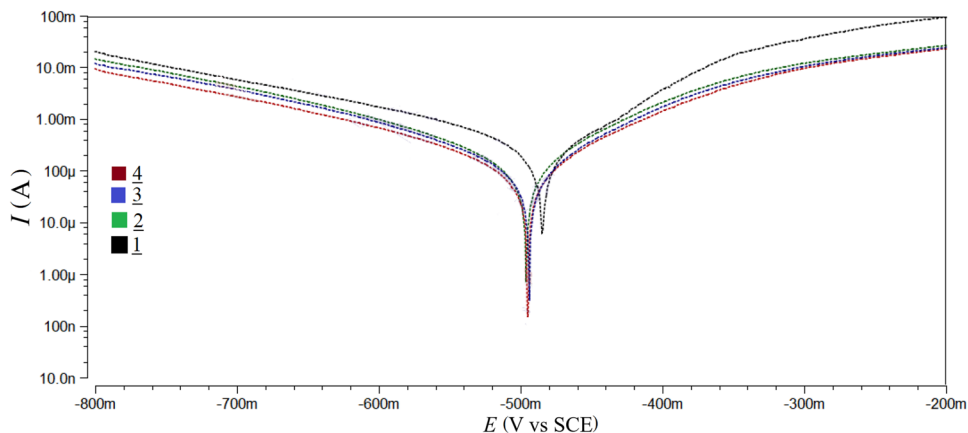
Table 1 Tafel curves results

Concentration (mg L^{-1})	$-E_{corr}$ (mV)	I_{corr} (µA cm^{-2})	β_a (± 1), (mV dec^{-1})	$-\beta_c$ (± 1) (mV dec^{-1})	θ ($\pm 10^{-2}$)	IE %
blank	470	1042	85	108	–	–
1	493	285	82	123	0.73	73
1.5	497	234	86	124	0.78	78
2	496	197	114	151	0.81	81

Fig. 4 Nyquist plots in the absence and presence of the corrosion inhibitor: blank (1), 1 (2), 1.5 (3), 2(4) mg L^{-1}

Table 2 AC impedance studies

Concentration (mg L^{-1})	R_s ($\pm 10^{-1}$) (Ω cm^2)	R_{ct} (± 1) (Ω cm^2)	Q_{dl} ($\pm 10^{-2}$) (mF cm^{-2})	C_{dl} ($\pm 10^{-2}$) (μF cm^{-2})	n ($\pm 10^{-2}$)
blank	1.1	4.99	210	0.214	0.76
1	1.3	12.8	122	0.141	0.76
1.5	1.4	19.8	137	0.196	0.75
2	1.3	21.5	143	0.208	0.75

electric charge (R_{ct}) increases and, consequently, the degree of corrosion of the steel in solution decreases. The plots show a depressed capacitive loop which arises from the time constant of the electrical double layer and charge transfer resistance. As can be seen, higher charge transfer resistance was obtained in the presence of the inhibitor. The data for the impedance test are shown in Table 2. As the inhibitor concentration increases, the amount of dual-layer capacitor (C_{dl}) decreases. This indicates that the inhibitory molecules replace the water molecules on the metal surface. Increasing the load transfer resistance and decreasing the capacitive hardness indicate that the charge transfer is a process that controls the corrosion of steel [43]. The results demonstrate that the presence of inhibitors enhance the value of R_{ct} obtained in the pure medium while that of Q_{dl} is reduced. The decrease in Q_{dl} values was caused by adsorption of inhibitor indicating that the exposed area decreased. On the other hand, a decrease in Q_{dl}, which can result from a decrease in local dielectric constant and/or an increase in the thickness of the electrical double layer, suggests that Schiff base inhibitors act by adsorption at the metal–solution interface. As the Q_{dl}, exponent (n) is a measure of the surface heterogeneity, values of n indicates that the steel surface becomes more and more homogeneous as the concentration of inhibitor increases as a result of its adsorption on the steel surface and corrosion inhibition. The increase in values of

R_{ct} and the decrease in values of Q_{dl} with increasing the concentration also indicate that Schiff bases act as primary interface inhibitors and the charge transfer controls the corrosion of steel under the open circuit conditions.

3.4 Adsorption Isotherm of the Corrosion Inhibitor

The main information on the interaction of the inhibitor with the surface of carbon steel can be obtained from the adsorption isotherm [47]. To obtain isotherms, it is necessary to find linear relationships between the values of the surface coverage (θ) and the inhibitor concentration (C_{inh}). Adsorption isotherms were tested for their fit to the experimental data. The linear regression coefficient values (R^2) are determined from the plotted curves. According to these results, it can be concluded that the best description of the adsorption behavior of three compounds can be explained by Langmuir adsorption isotherm. The Langmuir isotherm, in contrast to other isotherms, most fully described the adsorption behavior of the molecules of the studied inhibitors. According to this isotherm, θ is related to C_{inh} by the following equation [46]:

$$\frac{C_{inh}}{\theta} = C_{inh} + \frac{1}{K_{ads}} \tag{4}$$

where C_{inh} is the inhibitor concentration, *and* K_{ads} is the equilibrium constant of the adsorption process of the inhibitor.

According to Eq. 4, K_{ads} can be determined from the intersection point of the straight line on the graph of C_{inh}/θ versus C_{inh}. Also, the standard free energy of adsorption (ΔG°_{ads}) can be represented by the following equation [46]:

$$\Delta G^\circ_{ads} = -RT\ln(55.5K_{ads}) \tag{5}$$

where ΔG°_{ads} is the standard free energy of adsorption (J mol^{-1}), R is the universal gas constant (8.314 J mol^{-1} K^{-1}), and T is the temperature (K).

As shown in Fig. 5, the plot of C_{inh}/θ versus C_{inh} is a straight line, which depicts that the adsorption of all corrosion inhibitors on the surface of the carbon steel samples obeys the Langmuir isotherm. In this case, RSH was tested at 25 °C. The coefficient of determination (R^2) was practically equal to unity for all reagents. The high values of the coefficients of determination show that the surface of carbon steel samples was protected by the adsorption of inhibitor molecules, which fully corresponded to the Langmuir isotherm. Moreover, the equilibrium constant of the adsorption process (K_{ads}) is determined according to Eq. 4. The results are presented in Table 3. High K_{ads} values indicate that the inhibitor molecules have strong adsorption capacity on the surface of the carbon steel samples. The mixture of inhibitor had the highest K_{ads} value. In addition, the standard free
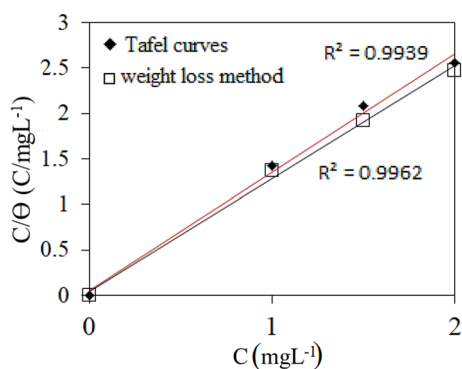
Fig. 5 Langmuir isotherm adsorption model RSH2 on the surface of steel in H_2SO_4 solution

**Table 3** The adsorption parameters of the corrosion inhibitor determined on the Langmuir isotherm

Method	R^2	K_{ads} (M)	ΔG°_{ads} (KJ mol^{-1})
Tafel curves	0.9962	894.7	− 32.35
weight loss	0.9939	878.9	− 32.03

energy of adsorption (ΔG°_{ads}) was calculated using Eq. 5 for the compound. The results are also shown in Table 3. Negative values of ΔG°_{ads} are consistent with the spontaneity of the adsorption process and the stability of the adsorbed layer on the surface of carbon steel samples. The values of ΔG°_{ads} for the corrosion inhibitor was around − 32 kJ mol^{-1}, which indicates that the adsorption mechanism on the surface of carbon steel in 0.5 M H_2SO_4 solution corresponds to the chemisorption of molecules.

The negative values of ΔG_{ads} suggest that the adsorption of Schiff bases on the carbon steel surface is spontaneous. Generally, the values of ΔG_{ads} around or less than − 30 kJ mol^{-1} are associated with the electrostatic interaction between charged molecules and the charged metal surface (physisorption), while those around or higher than − 40 kJ mol^{-1} mean charge sharing or transfer from the inhibitor molecules to the metal surface to form a coordinate type of metal bond (chemisorption). The values of K_{ads} and ΔG_{ads} are listed in Table 3. The ΔG_{ads} values are around − 30 kJ mol^{-1}, which means that the absorption of inhibitors on the carbon steel surface belongs to the physisorption and the adsorptive film has an electrostatic character [11–13].

3.5 Surface Morphology Study

The morphology of the surface of steel samples in half-molar acid solution was examined by AFM microscope in the presence of 2 mg RSH2 and without the inhibitor at 25 °C and after 24 h of immersion. The results are shown
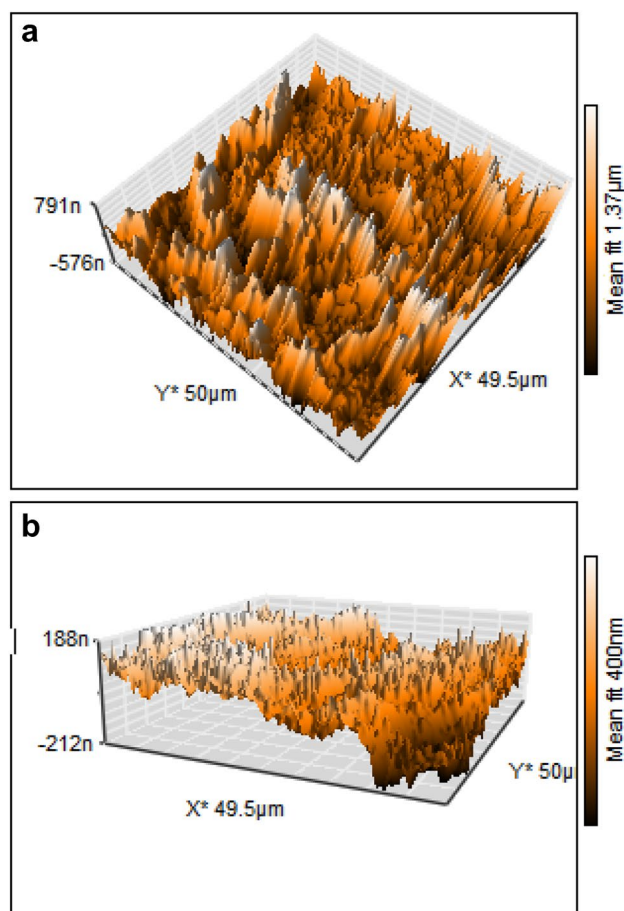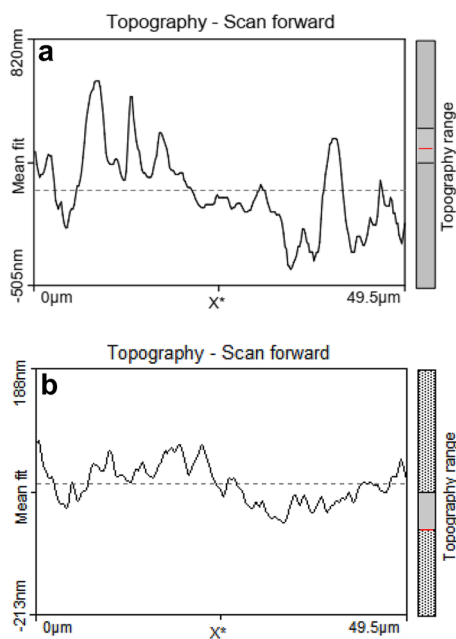

Fig. 6 **a** AFM images without corrosion inhibitor, **b** AFM images with corrosion inhibitor (3D View)

in Figs. 6 and 7. In the absence of inhibitor due to rapid corrosion by rough acid solution is observed. Corrosion in this case is relatively uniform and there is no sign of local corrosion. In the presence of the inhibitor, the steel surface roughness is reduced, which indicates the formation of a film on the metal surface and its inhibitory effect.

SEM images of abraded mild steel metal in 0.5 M H_2SO_4 solution without and with 2 mg L^{-1} of RSH2 is shown in the Fig. 8a and b. The surface of steel in the nonattendance of the inhibitor is highly corroded which is due to aggressive attack of sulfuric acid ions, whereas, in the presence of Schiff base compound, the significant enhancement in the steel surface smoothness was observed. This is due to adsorption of the inhibitor on the steel in 0.5 M H_2SO_4 solution.

3.6 DFT

The molecule's lowest thinkable beginning energy was gained by exploit a conformer search (Boltzmann jump technique; number of conformers: 3000; utilizing the COMPASS

Fig. 7 a AFM images without corrosion inhibitor, **b** AFM images with corrosion inhibitor (Line Graph)
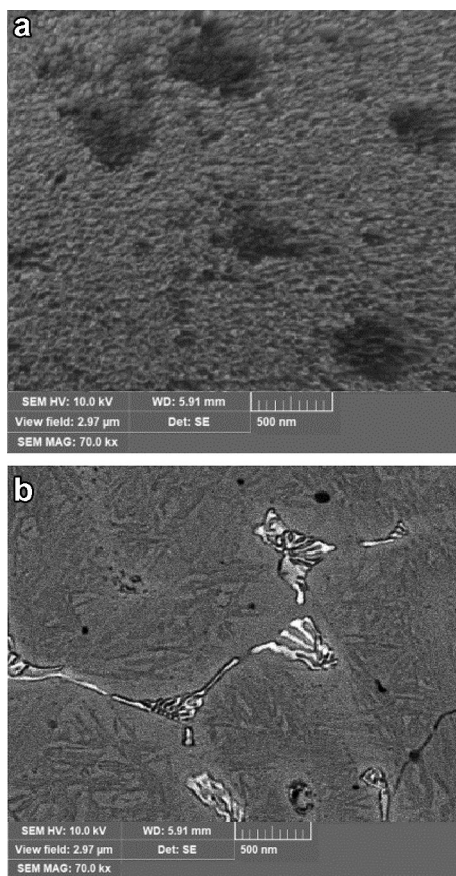
**Fig. 8 a** SEM images without corrosion inhibitor, **b** SEM images with corrosion inhibitor

II forcefield) during the early phase of the process. Figure 9 shows the lowest energy conformer which was used as the starting point for DFT calculations.

The σ-profile shows the charge density spreading on the molecule's surface and may be used to define the solubility of the inhibitor molecule (in our case water) [27, 29]. Utilizing the COSMO model's calculations allows for the generation of a charge density curve complete with a sigma profile. In COSMO, the electrostatic potential of atomic nuclei is represented by nuclei of atomic particles that have just a partial charge [28, 29, 48–50].

As can be seen in Fig. 10, inhibitor is capable of performing the dual role of H-bond acceptors and donors. When an inhibitor is dissolved, H-bond acceptor/donor associations are formed between water molecules, and the solubility of the inhibitor is controlled by its potential to establish H-bonds. O and N heteroatoms, which are located close to the HOMO electron density of the inhibitor, are also located close to the LUMO electron density, as is seen in Fig. 11. Figure 11 shows that the HOMO electron density is diffused toward the heteroatoms of the molecules (O and N) onto the phenyl ring, which suggests that these molecules are able to transmit electrons to the surface of the iron. This is something that can be seen in the figure. Coating of a protective organic layer on metal surfaces results from this electron sharing, which safeguards metal from corrosion [51–54]. LUMOs are electron acceptors that are related to sections of the inhibitor that get electrons from an electron surface that is rich in metals like that found in mild steel. These electrons come from an electron surface that has been enriched from a metal. LUMOs are electron acceptors that accept electrons from an electron surface that is rich in metals, such that found in mild steel. These electrons come from an electron surface that has a high concentration of metals [52, 53, 55, 56].

It is anticipated that surface adsorption will be marginally enhanced as a result of the exchange of lone pair electrons between heteroatoms (N and O) and the vacant iron d-orbital [47]. This will lead to a marginal increase in the surface absorption potential on the metal's surface. Surface adsorption will be somewhat amplified [52, 53, 57]. The most often reported qualifiers are included in Table 4, which is sorted by the frequency with which they have been used (the equations used to calculate them can be found elsewhere). It is feasible to obtain a better knowledge of the adsorptive behavior of inhibitors if one looks at the DFT simulations of inhibitors' adsorbing activities [54, 58, 59]. It is generally believed, in light of the inhibitors' low electron affinity and high ionization potential, that the adsorption of the inhibitors onto the Fe(110) surface is supported by the inhibitors' ability to exchange electrons with the metal surface. This is because the electron affinity of the inhibitors is high (Table 4) [38, 58, 60]. Chemical softness and hardness
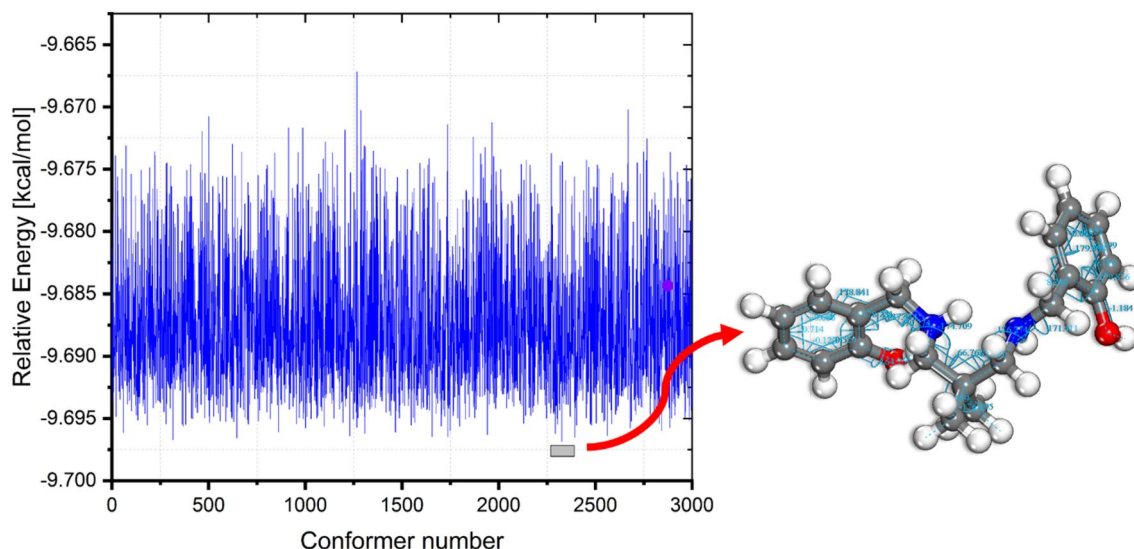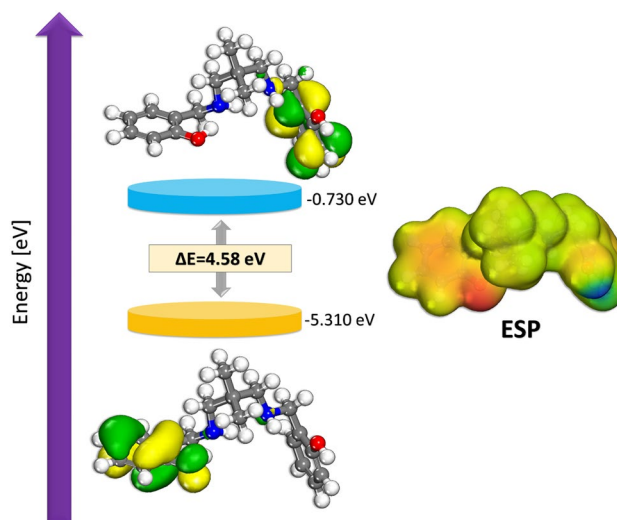
Fig. 9 Energies of the conformer search and the corresponding resulting structure of the inhibitor
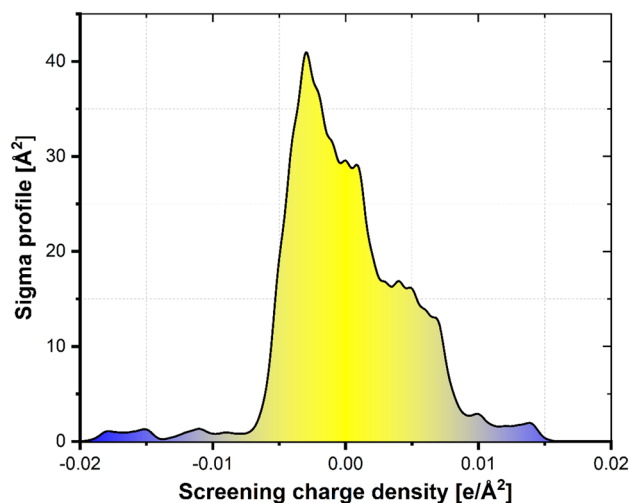
Fig. 10 σ-profile of the inhibitors

Fig. 11 HOMO, LUMO, and ESP surface of the inhibitor

are predicted values that represent the inhibitor's adsorption affinity for the metal surface, and high values of chemical softness are expected as a result of this adsorption affinity. The inhibitors ΔE is − 0.572, indicating that they have ability to accept electrons from the Fe(110) surface [38, 60–67].

When it comes to metal adsorption, Mulliken atomic charges (MAC) are a reliable and convincing indicator of the inhibitory sites (atoms) that are engaged in the process. A great number of suggestions have been put up in an effort to explain why a certain atom on the surface of Fe (1 1 0) and a variety of inhibitor chemicals are more likely to interact with one another [53, 54, 59]. Figure 12 is a representation of the inhibitor's MAC which is of particular importance to us. The oxygen and nitrogen atoms in inhibitor have very

negative charges, which indicate that these centers have the maximum density of electrons and, as a result, are the most effective in adhering to metallic surfaces. Inhibitors' oxygen and nitrogen atoms are responsible for the inhibition process. Figure 10 provides a visual representation of the molecular electrostatic potential (MEP) of the inhibitors at a range of different doses (area in red).

3.6.1 Monte Carlo and Molecular Dynamic Simulations

Starting with the Fe(110) surface as a point of departure makes it possible to calculate the adsorption energies of the system with a level of easiness that is comparable to that of

Table 4 Calculated theoretical chemical parameters for the inhibitor

Descriptor	Inhibitor
HOMO	− 5.3100
LUMO	− 0.7300
ΔE(HOMO–LUMO)	4.580
Ionization energy (I)	5.3100
Electron affinity A)	0.7300
Electronegativity (X)	3.0200
Global hardness (η)	2.2900
Chemical potential (π)	− 3.0200
Global softness (σ)	0.4367
Global electrophilicity (ω)	1.9914
Electrodonating (ω-) power	3.7876
Electroaccepting (ω+) power	0.7676
Net electrophilicity ($\Delta\omega$+-)	0.5036
Fraction of transferred electrons (ΔN)	0.0459
Energy from Inhb to Metals (ΔN)	0.0048
ΔE back-donation	− 0.5725
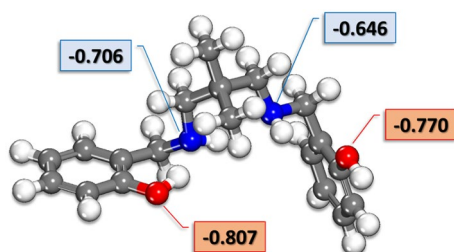
Fig. 12 Optimized structures of the inhibitors and their Mulliken atomic charges (MAC)

the calculation. The adsorption energy, also known as Eads, of a molecule may be determined with the use of the following equation [31, 32, 37, 38, 42, 43]:

$$E_{\text{adsorption}} = E_{\text{Fe(110)}_{||}\text{inhibitor}} - \left(\text{Fe}_{(110)} + E_{\text{inhibitor}}\right) \quad (6)$$

where $E_{\text{Fe(110)}_{||}\text{inhibitor}}$ is the total energy of the simulated system, E_{Fe}, and $E_{\text{inhibitor}}$ is the total energy of the Fe(110) surface and the corresponding free inhibitor molecules.

Following the fruitful conclusion of the MC calculations, a thorough investigation into the adsorption geometry of the inhibitor was carried out in order to validate the findings. A comparison of the values of the steady-state energy to the values of the starting energy may be used to evaluate the capability of the MC simulation to reach a state of equilibrium. The simulation had progressed to the point where the system had attained the condition of operation that required the least amount of energy. Figure 13 is a representation of the actual arrangement of the adsorbent inhibitors, which corresponds to the actual arrangement of the adsorbent inhibitors. This representation is made on a simulated Fe (110) plane. During the MD procedure, the surface of Fe (110) is decorated by the inhibitor in a direction that is virtually almost parallel to the inhibitor's orientation on the side of one of the phenyl rings. As seen in Fig. 9, we have a hypothesis that this adsorption pattern on the Fe (110) plane is caused by the backbone of an inhibitor molecule sticking to the surface atoms of the plane. This hypothesis is supported by the data (subject to the control of heteroatoms). The tendency of molecules to bring their heteroatoms and electron rings to the surface makes it possible for such molecules to adsorb, which is what gives those molecules their adsorptive properties [38, 52, 54, 65, 68].

The development of sizeable Eads (Fig. 14) on the surface of the metal is the consequence of inhibitors being adsorbed to the surface. Because of the exceptionally high adsorption energies of the inhibitor, it has a considerable adsorption interaction with the metal. The surface of the metal is protected against corrosion as a result of this behavior, which results in the formation of a protective layer on the metal's surface [52, 53, 55, 60, 61, 66, 68, 69]. MD is widely considered as a more accurate representation of the adsorption dynamics [39–41, 43].

After several hundreds of ps of NVT simulation, it is clear that the inhibitors shown in Fig. 13 adopt a somewhat planar geometry on both sides of the phenyl rings onto the metal surface. This results in a strong adsorption of the inhibitors onto the Fe surface. The RDF analysis of the MD trajectory obtained during corrosion simulations is a straightforward method that may be used to investigate the corrosion inhibitor adsorption on metal surfaces. This method is straightforward and doesn't involve any complications [54, 55, 59, 61].

If peaks emerge at a certain distance away from the metal surface, it is feasible to observe the adsorption processes that take place on metal surfaces by looking at the RDF graph [47, 67, 70]. When perceived in the 1–3.5 Å range in span, heights are regarded to be representative of chemisorbable processes; however, RDF peaks are ordinary to be present at distances higher than 3.5 Å in distance when representing physical adsorption processes. Numerous studies [47, 51, 55, 56, 59, 64, 68, 69] found that RDF peak values for Fe surface and inhibitor heteroatoms (N and O) were seen at distances smaller than 3.5 Å (Fig. 15). When the inhibitor interacts with the metal surface, it looks to be applying a significant interaction on it, as shown by its comparatively high negative energy value and RDF peaks. In our case, judging from the RDF graph, the inhibitor interacts with the Fe surface mainly through the O atoms.

Fig. 13 A. MC and B. MD poses the lowest adsorption configurations for inhibitors adsorption in the simulated corrosion media on the Fe (1 1 0) substrate
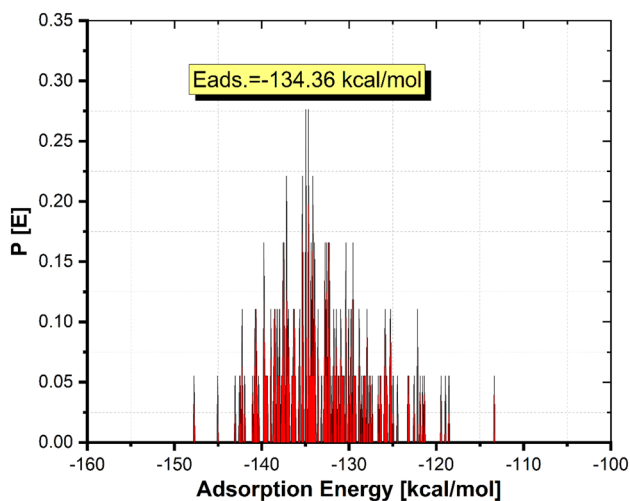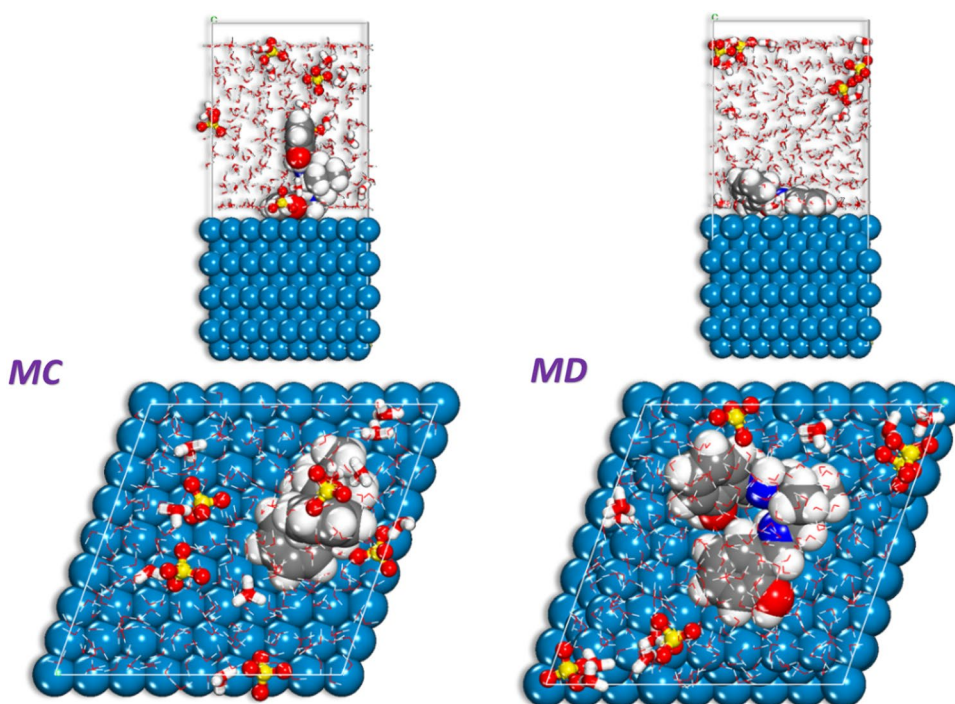
Fig. 14 The distribution of the adsorption energies of the inhibitors used in the simulated corrosion media obtained from MC calculations
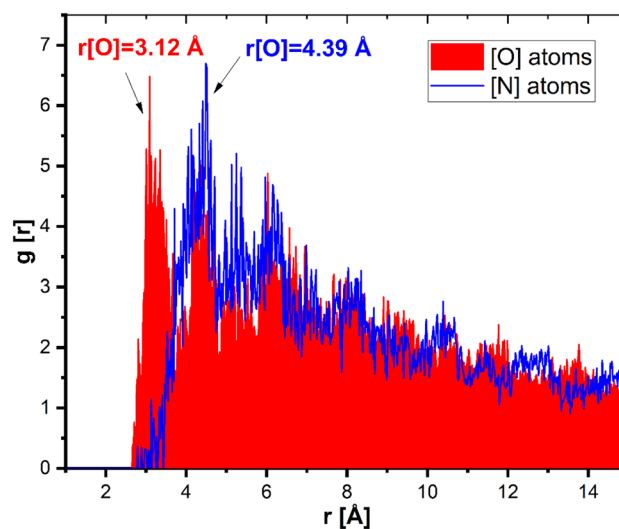
Fig. 15 RDF of heteroatoms (O and N) for the inhibitor on the Fe (110) surface accomplished from MD trajectory analysis

4 Conclusion

In this study, the effects of corrosion inhibition and the ability of adsorption of new compound (RSH2) on carbon steel surface were investigated and the following results were obtained. This organic compound has inhibition properties in 0.5 M H_2SO_4 medium. AFM analysis supports the creation of a preventive layer of inhibitor on steel surface layer which facilitates the lowering of corrosion rate. This inhibitor affects both anodic and cathodic branches and reduces the corrosion rate by reducing the exchange current of reactions by blocking existing sites. As a result of the MD calculations, it has been demonstrated that inhibitor is relatively flat-adsorbed on both sides of the phenyl rings, which result in the exposure of their adsorption centers to the surface of iron. The high negative adsorption energy of the inhibitor is supported also from experimental results.

Declarations

Conflict of interests The authors have no relevant financial or non-financial interests to disclose. On behalf of all authors, the corresponding author states that there is no conflict of interest.

References

1. İpekoğlu G, Küçükömeroğlu T, Aktarer SM, Sekban DM, Çam G (2019) Investigation of microstructure and mechanical properties of friction stir welded dissimilar St37/St52 joints. Mater Res Express 6:46537

2. Ebrahimnia M, Goodarzi M, Nouri M, Sheikhi M (2009) Study of the effect of shielding gas composition on the mechanical weld properties of steel ST 37–2 in gas metal arc welding. Mater Des 30:3891–3895. https://doi.org/10.1016/j.matdes.2009.03.031

3. Rajyalakshmi K, Rao BN (2019) Modified Taguchi approach to trace the optimum GMAW process parameters on weld dilution for ST-37 steel plates. J Test Eval 47:3209–3223

4. Fadaei A, Mokhtari H (2015) Finite element modeling and experimental study of residual stresses in repair butt weld of ST-37 plates. Iran J Sci Tech Trans Mech Eng 39:291

5. Khosrovaninezhad H, Shamanian M, Rezaeian A, Kangazian J, Nezakat M, Szpunar JA (2021) Insight into the effect of weld pitch on the microstructure-properties relationships of St 37/AISI 316 steels dissimilar welds processed by friction stir welding. Mater Charact 177:111188. https://doi.org/10.1016/j.matchar.2021.111188

6. Ghaderi M, Gerami M, Vahdani R (2020) Performance assessment of bolted extended end-plate moment connections constructed from grade St-37 steel subjected to fatigue. J Mater Civ Eng 32:04020092

7. Jafari H, Mohsenifar F, Sayin K (2016) Corrosion inhibition studies of N, N′-bis (4-formylphenol)-1, 2-Diaminocyclohexane on steel in 1 HCl solution acid. J Taiwan Inst Chem Eng 64:314–324. https://doi.org/10.1016/j.jtice.2016.04.021

8. Jafari H, Sayin K (2015) Electrochemical and theoretical studies of adsorption and corrosion inhibition of aniline violet compound on carbon steel in acidic solution. J Taiwan Inst Chem Eng 56:181–190. https://doi.org/10.1016/j.jtice.2015.03.030

9. Jafari H, Danaee I, Eskandari H, RashvandAvei M (2014) Combined computational and experimental study on the adsorption and inhibition effects of N_2O_2 schiff base on the corrosion of API 5L grade B steel in 1 mol/L HCl. J Mater Sci Technol 30:239–252. https://doi.org/10.1016/j.jmst.2014.01.003

10. Jafari H, Danaee I, Eskandari H, RashvandAvei M (2013) Electrochemical and theoretical studies of adsorption and corrosion inhibition of N, N′-bis (2-hydroxyethoxyacetophenone)-2, 2-dimethyl-1, 2-propanediimine on low carbon steel (API 5L Grade B) in acidic solution. Ind Eng Chem Res 52:6617–6632. https://doi.org/10.1021/ie400066x

11. Ameri E, Jafari H, Rezaeevala M, Vakili MH, Mokhtarian N (2022) Synthesized Schiff base acted as eco-friendly inhibitor for mild steel in 1N H_2SO_4. Chem Rev Lett 5:119–126. https://doi.org/10.22034/crl.2022.328744.1153

12. Fouda AS, Abdallah M, Medhat M (2012) Some Schiff base compounds as inhibitors for corrosion of carbon steel in acidic media.

13. Rezaeivala M, Karimi S, Sayin K, Tüzün B (2022) Experimental and theoretical investigation of corrosion inhibition effect of two piperazine-based ligands on carbon steel in acidic media. Colloids Surf A 641:128538. https://doi.org/10.1016/j.colsurfa.2022.128538

14. Jafari H, Ameri E, Rezaeivala M (2021) Investigation of adsorption of new Schiff base on steel surface in sulfuric acid medium. Farayandno 16:16–26

15. Al-Gorair AS, Abdallah M (2021) Expired paracetamol as corrosion inhibitor for low carbon steel in sulfuric acid. Electrochemical, kinetics and thermodynamics investigation. Int J Electrochem Sci 16:210771

16. Barmatov E, Hughes T (2021) Degradation of a schiff-base corrosion inhibitor by hydrolysis, and its effects on the inhibition efficiency for steel in hydrochloric acid. Mater Chem Phys 257:123758. https://doi.org/10.1016/j.matchemphys.2020.123758

17. Zhang Y, Pan Y, Li P, Zeng X, Guo B, Pan J, Hou L, Yin X (2021) Novel Schiff base-based cationic Gemini surfactants as corrosion inhibitors for Q235 carbon steel and printed circuit boards. Colloids Surf A 623:126717. https://doi.org/10.1016/j.colsurfa.2021.126717

18. Satpati S, Suhasaria A, Ghosal S, Saha A, Dey S, Sukul D (2021) Amino acid and cinnamaldehyde conjugated Schiff bases as proficient corrosion inhibitors for mild steel in 1 M HCl at higher temperature and prolonged exposure: detailed electrochemical, adsorption and theoretical study. J Mol Liq 324:115077. https://doi.org/10.1016/j.molliq.2020.115077

19. Jafari H, Ameri E, Rezaeivala M, Berisha A, Halili J (2022) Anti-corrosion behavior of two N_2O_4 Schiff-base ligands: experimental and theoretical studies. J Phys Chem Solids 164:110645. https://doi.org/10.1016/j.jpcs.2022.110645

20. Karimi S, Rezaeivala M, Sayin K, Tuzun B (2022) Experimental and computational investigation of 3, 5-di-tert-butyl-2-(((3-((2-morpholinoethyl)(pyridin-2-ylmethyl) amino) propyl) imino) methyl) phenol and related reduced form as an inhibitor for C-steel. Mater Chem Phys. https://doi.org/10.1016/j.matchemphys.2022.126152

21. Rezaeivala M, Karimi S, Tuzun B, Sayin K (2022) Anti-corrosion behavior of 2-((3-(2-morpholino ethylamino)-N3-((pyridine-2-yl) methyl) propylimino) methyl) pyridine and its reduced form on carbon steel in hydrochloric acid solution: experimental and theoretical studies. Thin Solid Films 741:139036. https://doi.org/10.1016/j.tsf.2021.139036

22. Jafari H, Akbarzade K, Danaee I (2019) Corrosion inhibition of carbon steel immersed in a 1 M HCl solution using benzothiazole derivatives. Arabian J Chem 12:1387–1394. https://doi.org/10.1016/j.arabjc.2014.11.018

23. Zhao Y, Truhlar DG (2008) The M06 suite of density functionals for main group thermochemistry, thermochemical kinetics, non-covalent interactions, excited states, and transition elements: two new functionals and systematic testing of four M06-class functionals and 12 other functionals. Theor Chem Acc 120:215–241. https://doi.org/10.1007/s00214-007-0310-x

24. Ben Hadj Ayed M, Osmani T, Issaoui N, Berisha A, Oujia B, Ghalla H (2019) Structures and relative stabilities of Na+ Nen (n= 1–16) clusters via pairwise and DFT calculations. Theor Chem Acc 138:84. https://doi.org/10.1007/s00214-019-2476-4

25. Mardirossian N, Head-Gordon M (2017) Thirty years of density functional theory in computational chemistry: an overview and extensive assessment of 200 density functionals. Mol Phys 115:2315–2372. https://doi.org/10.1080/00268976.2017.1333644

26. Inada Y, Orita H (2008) Efficiency of numerical basis sets for predicting the binding energies of hydrogen bonded complexes: evidence of small basis set superposition error compared to

Prot Met Phys Chem 48:477–486. https://doi.org/10.1134/S2070205112040053

Gaussian basis sets. J Comput Chem 29:225–232. https://doi.org/10.1002/jcc.20782

27. Klamt K (2005) COSMO-RS: from quantum chemistry to fluid phase thermodynamics and drug design. Elsevier, Amsterdam

28. Klamt K (2018) The COSMO and COSMO-RS solvation models. Wiley Interdiscip Rev Comput Mol Sci 8:1338. https://doi.org/10.1002/wcms.1338

29. Berisha A (2019) Interactions between the aryldiazonium cations and graphene oxide: a DFT study. J Chem. https://doi.org/10.1155/2019/5126071

30. Dagdag O, Berisha A, Mehmeti V, Haldhar R, Berdimurodov E, Hamed O, Jodeh S, Lgaz H, Sherif ESM, Ebenso EE (2021) Epoxy coating as effective anti-corrosive polymeric material for aluminum alloys: formulation, electrochemical and computational approaches. J Mol Liq. https://doi.org/10.1016/J.MOL-LIQ.2021.117886

31. Ouass A, Galai M, Ouakki M, Ech-Chihbi E, Kadiri L, Hsissou R, Essaadaoui Y, Berisha A, Cherkaoui M, Lebkiri A, Rifi EA (2021) Poly(sodium acrylate) and Poly(acrylic acid sodium) as an eco-friendly corrosion inhibitor of mild steel in normal hydrochloric acid: experimental, spectroscopic and theoretical approach. J Appl Electrochem 517(51):1009–1032. https://doi.org/10.1007/S10800-021-01556-Y

32. Dagdag O, El Harfi A, El Gana L, Safi ZS, Guo L, Berisha A, Verma C, Ebenso EE, Wazzan N, Gouri ME (2021) Designing of phosphorous based highly functional dendrimeric macromolecular resin as an effective coating material for carbon steel in NaCl: computational and experimental studies. J Appl Polym Sci 138:49673. https://doi.org/10.1002/APP.49673

33. Faydy ME, About H, Warad I, Kerroum Y, Berisha A, Podvorica F, Bentiss F, Kaichouh G, Lakhrissi B, Zarrouk A (2021) Insight into the corrosion inhibition of new bis-quinolin-8-ols derivatives as highly efficient inhibitors for C35E steel in 0.5 M H₂SO₄. J Mol Liq 342:117333. https://doi.org/10.1016/J.MOL-LIQ.2021.117333

34. Molhi A, Hsissou R, Damej M, Berisha A, Thaçi V, Belafhaili A, Benmessaoud M, Labjar N, Hajjaj SE (2021) Contribution to the corrosion inhibition of c38 steel in 1 m hydrochloric acid medium by a new epoxy resin pgeppp. Int J Corros Scale Inhib. 10:399–418

35. Alahiane M, Oukhrib R, Berisha A, Albrimi YA, Akbour RA, Oualid HA, Bourzi H, Assabbane A, Nahlé A, Hamdani M (2021) Electrochemical, thermodynamic and molecular dynamics studies of some benzoic acid derivatives on the corrosion inhibition of 316 stainless steel in HCl solutions. J Mol Liq 328:115413. https://doi.org/10.1016/J.MOLLIQ.2021.115413

36. Uppalapati PK, Berisha A, Velmurugan K, Nandhakumar R, Khosla A, Liang T (2021) Salen type additives as corrosion mitigator for Ni–W alloys: detailed electronic/atomic-scale computational illustration. Int J Quantum Chem 121:1–8. https://doi.org/10.1002/QUA.26600

37. Haldhar R, Prasad D, Bahadur I, Dagdag O, Berisha A (2021) Evaluation of Gloriosa superba seeds extract as corrosion inhibition for low carbon steel in sulfuric acidic medium: a combined experimental and computational studies. J Mol Liq 323:114958. https://doi.org/10.1016/J.MOLLIQ.2020.114958

38. Guo L, Qi C, Zheng X, Zhang R, Shen X, Kaya S (2017) Toward understanding the adsorption mechanism of large size organic corrosion inhibitors on an Fe(110) surface using the DFTB method. RSC Adv 7:29042–29050. https://doi.org/10.1039/C7RA04120A

39. Mehmeti V (2022) Nystatin drug as an effective corrosion inhibitor for mild steel in acidic media–an experimental and theoretical study. Corros Sci Technol. 21:21–31

40. Sayin K, Jafari H (2016) Effect of pyridyl on adsorption behavior and corrosion inhibition of aminotriazole. J Taiwan Inst Chem Eng 68:431–439. https://doi.org/10.1016/j.jtice.2016.08.036

41. Jafari H, Danaee I, Eskandari H (2015) Inhibitive action of novel Schiff base towards corrosion of API 5L carbon steel in 1 M hydrochloric acid solutions. Trans Indian Inst Met 68:729–739. https://doi.org/10.1007/s12666-014-0506-4

42. Mohsenifar F, Jafari H, Sayin K (2016) Investigation of thermodynamic parameters for steel corrosion in acidic solution in the presence of N,N′-Bis (phloroacetophenone)-1,2 propanediamine. J Bio Tribo Corros 2:1–3. https://doi.org/10.1007/s40735-015-0031-y

43. Haldhar R, Prasad D, Nguyen LT, Kaya S, Bahadur I, Dagdag O, Kim SC (2021) Corrosion inhibition, surface adsorption and computational studies of Swertia chirata extract: a sustainable and green approach. Mater Chem Phys 267:124613. https://doi.org/10.1016/j.matchemphys.2021.124613

44. He J, Xu Q, Li G, Li Q, Marzouki R, Li W (2021) Insight into the corrosion inhibition property of *Artocarpus heterophyllus* Lam leaves extract. J Ind Eng Chem 102:260–270. https://doi.org/10.1016/j.jiec.2021.07.007

45. Jafari H, Danaee I, Eskandari H, Rashvandavei M (2013) Electrochemical and quantum chemical studies of N, N′-bis (4-hydroxybenzaldehyde)-2, 2-dimethylpropandiimine Schiff base as corrosion inhibitor for low carbon steel in HCl solution. J Environ Sci Health Part A 48:1628–1641. https://doi.org/10.1080/10934529.2013.815094

46. Umoren SA, Suleiman RK, Obot IB, Solomon MM, Adesina AY (2022) Elucidation of corrosion inhibition property of compounds isolated from Butanolic Date Palm leaves extract for low carbon steel in 15% HCl solution: experimental and theoretical approaches. J Mol Liq 8:119002. https://doi.org/10.1016/j.molliq.2022.119002

47. Shahmoradi AR, Talebibahmanbigloo N, Nickhil C, Nisha R, Javidparvar AA, Ghahremani P, Bahlakeh G, Ramezanzadeh B (2022) Molecular-MD/atomic-DFT theoretical and experimental studies on the quince seed extract corrosion inhibition performance on the acidic-solution attack of mild-steel. J Mol Liq 346:117921. https://doi.org/10.1016/j.molliq.2021.117921

48. Berisha A (2019) The influence of the grafted aryl groups on the solvation properties of the graphyne and graphdiyne—a MD study. Open Chem 17:703–710. https://doi.org/10.1515/chem-2019-0083

49. Ongari D, Boyd PG, Kadioglu O, Mac AK, Keskin ES, Smit B (2019) Evaluating charge equilibration methods to generate electrostatic fields in nanoporous materials. J Chem Theory Comput 15:382–401. https://doi.org/10.1021/acs.jctc.8b00669

50. Hsissou R, Benhiba F, About S, Dagdag O, Benkhaya S, Berisha A, Erramli H, Elharfi A (2020) Trifunctional epoxy polymer as corrosion inhibition material for carbon steel in 1.0 M HCl: MD simulations, DFT and complexation computations. Inorg Chem Commun. https://doi.org/10.1016/j.inoche.2020.107858

51. Dagdag O, Berisha A, Safi Z, Hamed O, Jodeh S, Verma C, Ebenso EEE, Harfi AE (2020) DGEBA-polyaminoamide as effective anti-corrosive material for 15CDV6 steel in NaCl medium: computational and experimental studies. J Appl Polym Sci 137:48402. https://doi.org/10.1002/app.48402

52. Mehmeti VV, Berisha AR (2017) Corrosion study of mild steel in aqueous sulfuric acid solution using 4-methyl-4h-1,2,4-triazole-3-thiol and 2-mercaptonicotinic acid-an experimental and theoretical study. Front Chem. https://doi.org/10.3389/FCHEM.2017.00061

53. Dagdag O, Hsissou R, Harfi AE, Berisha A, Safi Z, Verma C, Ebenso EEE, Touhami ME, Gouri ME (2020) Fabrication of polymer based epoxy resin as effective anti-corrosive coating for steel: computational modeling reinforced experimental studies. Surf Interfaces 18:100454. https://doi.org/10.1016/j.surfin.2020.100454

54. Hsissou R, Dagdag O, About S, Benhiba F, Berradi M, Bouchti ME, Berisha A, Hajjaji N, Elharfi A (2019) Novel derivative

epoxy resin TGETET as a corrosion inhibition of E24 carbon steel in 1.0 M HCl solution. Experimental and computational (DFT and MD simulations) methods. J Mol Liq 284:182–192. https://doi.org/10.1016/j.molliq.2019.03.180

55. Berisha A, Podvorica F, Mehmeti V, Syla F, Vataj D (2015) Theoretical and experimental studies of the corrosion behavior of some thiazole derivatives toward mild steel in sulfuric acid media. Maced J Chem Chem Eng 34:287–294

56. Fouda AS, Ellithy AS (2009) Inhibition effect of 4-phenylthiazole derivatives on corrosion of 304L stainless steel in HCl solution. Corros Sci 51:868–875. https://doi.org/10.1016/j.corsci.2009.01.011

57. Dagdag O, Berisha A, Safi Z, Dagdag S, Berrani M, Jodeh S, Verma C, Ebenso EEE, Wazzan N, Harfi AE (2020) Highly durable macromolecular epoxy resin as anticorrosive coating material for carbon steel in 3% NaCl: computational supported experimental studies. J Appl Polym Sci. https://doi.org/10.1002/app.49003

58. Hsissou R, About S, Seghiri R, Rehioui M, Berisha A, Erramli H, Assouag M, Elharfi A (2020) Evaluation of corrosion inhibition performance of phosphorus polymer for carbon steel in [1 M] HCl: computational studies (DFT, MC and MD simulations). J Mater Res Technol. https://doi.org/10.1016/j.jmrt.2020.01.002

59. Dagdag O, Hsissou R, Berisha A, Erramli H, Hamed O, Jodeh S, Harfi AE (2019) Polymeric-based epoxy cured with a polyaminoamide as an anticorrosive coating for aluminum 2024–T3 surface: experimental studies supported by computational modeling. J Bio-Tribo-Corrosion. https://doi.org/10.1007/s40735-019-0251-7

60. Jessima SJHMHM, Berisha A, Srikandan SSSS, Subhashini S (2020) Preparation, characterization, and evaluation of corrosion inhibition efficiency of sodium lauryl sulfate modified chitosan for mild steel in the acid pickling process. J Mol Liq 320:114382. https://doi.org/10.1016/j.molliq.2020.114382

61. Jessima SJHM, Berisha A, Srikandan SS, Subhashini S (2020) Preparation, characterization, and evaluation of corrosion inhibition efficiency of sodium lauryl sulfate modified chitosan for mild steel in the acid pickling process. J Mol Liq. https://doi.org/10.1016/j.molliq.2020.114382

62. Guo L, Zhang ST, Li WP, Hu G, Li X (2014) Experimental and computational studies of two antibacterial drugs as corrosion inhibitors for mild steel in acid media. Mater Corros 65:935–942. https://doi.org/10.1002/maco.201307346

63. Hsissou R, Benzidia B, Rehioui M, Berradi M, Berisha A, Assouag M, Hajjaji N, Elharfi A (2020) Anticorrosive property of hexafunctional epoxy polymer HGTMDAE for E24 carbon steel corrosion in 1.0 M HCl: gravimetric, electrochemical, surface morphology and molecular dynamic simulations. Polym Bull 77:3577–3601. https://doi.org/10.1007/s00289-019-02934-5

64. Dagdag O, Hsissou R, Harfi AE, Safi Z, Berisha A, Verma C, Ebenso EE, Quraishi MA, Wazzan N, Jodeh S, Gouri ME (2020) Epoxy resins and their zinc composites as novel anti-corrosive materials for copper in 3% sodium chloride solution: experimental and computational studies. J Mol Liq 315:113757. https://doi.org/10.1016/j.molliq.2020.113757

65. Rbaa M, Dohare P, Berisha A, Dagdag O, Lakhrissi L, Galai M, Lakhrissi B, Touhami ME, Warad I, Zarrouk A (2020) New Epoxy sugar based glucose derivatives as eco friendly corrosion inhibitors for the carbon steel in 1.0 M HCl: experimental and theoretical investigations. J Alloys Compd 833:154949. https://doi.org/10.1016/j.jallcom.2020.154949

66. Yu LJ, Zhang J, Qiao GM, Yan YG, Ti Y, Zhang Y (2013) Effect of alkyl chain length on inhibition performance of imidazoline derivatives investigated by molecular dynamics simulation. Mater Corros 64:225–230. https://doi.org/10.1002/maco.201106141

67. Berisha A (2022) An experimental and theoretical investigation of the efficacy of pantoprazole as a corrosion inhibitor for mild steel in an acidic medium. Electrochem 3:28–41. https://doi.org/10.3390/ELECTROCHEM3010002

68. About S, Zouarhi M, Chebabe D, Damej M, Berisha A, Hajjaji N (2020) Galactomannan as a new bio-sourced corrosion inhibitor for iron in acidic media. Heliyon 6:3574. https://doi.org/10.1016/j.heliyon.2020.e03574

69. Hsissou R, About S, Berisha A, Berradi M, Assouag M, Hajjaji N, Elharfi A (2019) Experimental, DFT and molecular dynamics simulation on the inhibition performance of the DGDCBA epoxy polymer against the corrosion of the E24 carbon steel in 1.0 M HCl solution. J Mol Struct 1182:340–351. https://doi.org/10.1016/j.molstruc.2018.12.030

70. Bhardwaj N, Sharma P, Berisha A, Mehmeti V, Dagdag O, Kumar V (2022) Monte Carlo simulation, molecular dynamic simulation, quantum chemical calculation and anti-corrosive behaviour of *Citrus limetta* pulp waste extract for stainless steel (SS-410) in acidic medium. Mater Chem Phys 284:126052. https://doi.org/10.1016/J.MATCHEMPHYS.2022.126052